European Journal of Radiology Open 9 (2022) 100421

Contents lists available at ScienceDirect

European Journal of Radiology Open

journal homepage: www.elsevier.com/locate/ejro

Impact of acceleration on bone depiction quality by ultrashort echo time magnetic resonance bone imaging sequences in medication-related osteonecrosis of the jaw

Jonas M. Getzmann [a,b,*,1], Florian A. Huber [a,b,1], Dominik Nakhostin [a,b], Eva Deininger-Czermak [a,b,e], Paul Schumann [b,c], Tim Finkenstaedt [a,b], Filippo Del Grande [d], Roman Guggenberger [a,b]

[a] Institute of Diagnostic and Interventional Radiology, University Hospital Zurich (USZ), Raemistrasse 100, CH-8091 Zurich, Switzerland
[b] University of Zurich (UZH), Raemistrasse 100, CH-8091 Zurich, Switzerland
[c] Department of Cranio-Maxillo-Facial and Oral Surgery, University Hospital Zurich (USZ), Raemistrasse 100, CH-8091 Zurich, Switzerland
[d] EOC Clinic of Radiology, Imaging Institute of Southern Switzerland (IIMSI), Via Tesserete 46, CH-6900 Lugano, Switzerland
[e] Institute of Forensic Medicine, University of Zurich (UZH), Winterthurerstrasse 190/52, CH-8057 Zurich, Switzerland

HIGHLIGHTS

- Ultrashort echo time MRI can assess medication-related osteonecrosis of the jaw.
- Sequences with a lower number of radial acquisitions reduce scan times.
- Image quality for detecting bony changes remains sufficient.

ARTICLE INFO

Keywords:
Medication-related osteonecrosis of the jaw
Magnetic resonance imaging
Ultrashort echo time

ABSTRACT

Objectives: To assess the impact on bone depiction quality by decreasing number of radial acquisitions (RA) of a UTE MR bone imaging sequence in MRONJ.
Material and methods: UTE MR bone imaging sequences using pointwise encoding time reduction with RA (PETRA) with 60'000, 30'000 and 10'000 RA were acquired in 16 patients with MRONJ and 16 healthy volunteers. Blinded readout sessions were performed by two radiologists. Qualitative analysis compared the detection of osteolytic lesions and productive bony changes in the PETRA sequences of the patients with MRONJ. Quantitative analysis assessed the differences in image artifacts, contrast-to-noise ratio (CNR) and image noise.
Results: Acquisition times were reduced from 315 to 165 and 65 s (60'000, 30'000, 10'000 RA, respectively), resulting in a fewer number of severe motion artifacts. Bone delineation was increasingly blurred when reducing the number of RA but without any trade-off in terms of diagnostic performance. Interreader agreement for the detection of pathognomonic osteolysis was moderate ($\kappa = 0.538$) for 60'000 RA and decreased to fair ($\kappa = 0.227$ and $\kappa = 0.390$) when comparing 30'000 and 10'000 RA, respectively. Image quality between sequences was comparable regarding CNR, image noise and artifact dimensions without significant differences (all $P > 0.05$).
Conclusions: UTE MR bone imaging sequences with a lower number of RA provide sufficient image quality for detecting osteolytic lesions and productive bony changes in MRONJ subjects at faster acquisition times compared to the respective standard UTE MR bone imaging sequence.

* Correspondence to: Institute of Diagnostic and Interventional Radiology, University Hospital Zurich (USZ), University of Zurich (UZH), Raemistrasse 100, CH-8091 Zurich, Switzerland.
E-mail address: jonas.getzmann@usz.ch (J.M. Getzmann).
[1] shared first authorship

https://doi.org/10.1016/j.ejro.2022.100421
Received 1 March 2022; Received in revised form 7 April 2022; Accepted 13 April 2022

1. Introduction

Medication-related osteonecrosis of the jaw (MRONJ) is an adverse side effect traditionally observed in patients treated with antiresorptive drugs such as bisphosphonates (BP) or denosumab. These drugs are used to preserve and strengthen existing bone in osteoporosis, to manage cancer-related conditions including hypercalcemia of malignancy, and to prevent skeletal-related events associated with bone metastases of solid malignant tumors [1–5]. Regardless of indications for therapy, the duration and dosage of BP or antiresorptive therapy is a risk factor for developing MRONJ [6,7].

To distinguish MRONJ from other delayed healing conditions, the American Association of Oral and Maxillofacial Surgeons (AAOMS) has defined the following diagnostic criteria: (1) current or previous treatment with antiresorptive or antiangiogenic drugs; (2) exposed bone or positive bone-probing intra- or extraoral fistula for more than 8 weeks; and (3) no history of radiation therapy to the jaws [1].

Even though the diagnosis of MRONJ depends on patient history and clinical features, imaging is essential to determine the extent of disease and diagnose early stages by detecting subtle osteolytic lesions or productive bony changes (e.g., medullary osteosclerosis or periosteal thickening) [8,9]. In general practice, suspected cases of MRONJ are first assessed using X-ray-based modalities such as panoramic radiographs (PRs) or cone-beam computed tomography (CBCT) with the latter having the advantage of a high isotropic spatial resolution allowing for detailed analysis of bony structures [10,11]. However, CBCT performs poorly in assessing potential soft tissue involvement and/or nerve integrity which may be important in more advanced stages of MRONJ [12].

More recently, ultrashort echo time (UTE) MR sequences have been introduced and applied clinically to detect structures with very short echo times such as tendons and bones [13–15]. With regard to MRONJ, a recent study has also shown results comparable to CBCT regarding qualitative assessment of bone changes when using an UTE MR bone imaging sequence using pointwise encoding time reduction with radial acquisition (RA) (PETRA, Siemens Healthineers, Erlangen, Germany) [14,16]. However, MR imaging is susceptible to motion artifacts which is why shorter acquisition times are generally desirable, especially in the predominantly older MRONJ patient population [17]. The number of views in a radially acquired sequence in order to sample the entire k-space directly correlates with acquisition time [18]. Image quality is compromised when reducing RA, however, diagnostic capabilities with regard to detection and classification of MRONJ associated bone changes may remain largely preserved.

The aim of this study was to assess the impact on bone depiction quality by decreasing number of RA of a specific UTE MR bone imaging sequence (i.e. PETRA) in MRONJ.

2. Material and methods

2.1. Patient population

Patients with clinically confirmed MRONJ according to the AAOMS diagnostic criteria [1] who were assessed with MR imaging at our institution between December 2018 and September 2019 were prospectively included in the study (6 males, 10 females, age 67.7 ± 12.9 years (mean ± SD)). All patients diagnosed with MRONJ who had undergone oral surgery before the date of MR imaging were excluded. All MRONJ foci were eventually confirmed by histology. In addition, a control group of 16 healthy volunteers (8 males, 8 females, age 24.5 ± 2.9 years (mean ± SD)) was recruited to undergo MR imaging of the jaws.

Data search was performed with the institutional PACS systems (synedra View; synedra information technologies Ltd, Innsbruck, Austria; and IMPAX 6; Agfa-Gevaert N.V., Mortsel, Belgium) and the hospital information system (KISIM, Version 5.2.0.10; CISTEC AG, Zurich, Switzerland).

The study was approved by the institutional review board and the local ethics committee (BASEC-Nr. 2018–01752) and conducted in accordance with the principles of the Declaration of Helsinki. Written general consent for the use of clinical data for scientific purposes was obtained from each patient.

2.2. Magnetic resonance imaging

MR imaging was performed with a 3.0 Tesla scanner (MAGNETOM Skyra; Siemens Healthineers, Erlangen, Germany) by using a dedicated 64-channel head coil. The institution's standard MR protocol for assessing osteonecrosis of the jaw was applied including axial and coronal T1-weighted turbo spin echo (TSE) sequences, an axial fat-saturated, fluid-sensitive turbo inversion recovery magnitude (TIRM) sequence, and a diffusion-weighted sequence.

After intravenous administration of a gadolinium-based contrast agent (Gadovist; Bayer AG, Leverkusen, Germany), all MRONJ patients were additionally scanned with an axial T1-weighted fat-saturated TSE sequence. The 16 volunteers of the control group did not receive any contrast agent.

For UTE MR bone imaging, standard (60'000 RA), fast (30'000 RA), and ultra-fast (10'000 RA) PETRA sequences were obtained in both groups either at the beginning or at the end of the standard non-contrast-enhanced MR sequences (Table 1).

2.3. Qualitative analysis

Qualitative analysis of the different image series in the group of patients with clinically confirmed MRONJ was independently performed by two radiologists with 3 and 13 years of MR experience, respectively. The standard PETRA sequence was assessed first with regard to osteolysis (cortical discontinuity/sequester), periosteal thickening (hypointense thickening of the jaw cortex), and medullary osteosclerosis (diffuse hypointensity of the bone marrow) [8,9]. Grading was performed by using a 4-point Likert scale [19] (0–3, for "normal findings", "mild pathology", "moderate pathology", and "severe pathology", Fig. 1) in five predefined anatomic regions in the mandible and two predefined regions in the maxilla on each side as published previously: anterior corpus of mandible (aMa, between mental foramina), posterior corpus of mandible (pMa, between mental foramen and angle of the mandible), ramus mandibularis (rMa), condyloid process of mandible (conMa), coronoid process of mandible (corMa), anterior maxilla (aMx) and posterior maxilla (pMx) [14,20].

Motion artifacts throughout the entire jaw region were assessed separately and rated using the same 4-point Likert scale. Anatomic regions with severe artifacts leading to non-diagnostic image quality were

Table 1
Image acquisition parameters of the PETRA sequences based on different number of radial acquisitions.

	Standard PETRA	Fast PETRA	Ultra-fast PETRA
Radial acquisitions	60'000	30'000	10'000
Acquisition time	315 s	165 s	65 s
Field strength	3.0 T	3.0 T	3.0 T
Voxel size	0.70 mm^3	0.70 mm^3	0.70 mm^3
Slice thickness	0.7 mm	0.7 mm	0.7 mm
TE	0.07 ms	0.07 ms	0.07 ms
TR	5 ms	5 ms	5 ms
Field of view	246 × 246 mm	246 × 246 mm	246 × 246 mm
Coil	64-channel head	64-channel head	64-channel head
Base resolution	352	352	352
Bandwidth	355 Hz/Px	355 Hz/Px	355 Hz/Px

PETRA indicates pointwise encoding time reduction with radial acquisition; Standard, fast and ultra-fast PETRA refers to the UTE MR bone imaging sequences with 60'000, 30'000 and 10'000 radial acquisitions, respectively; TE, echo time; TR, repetition time.

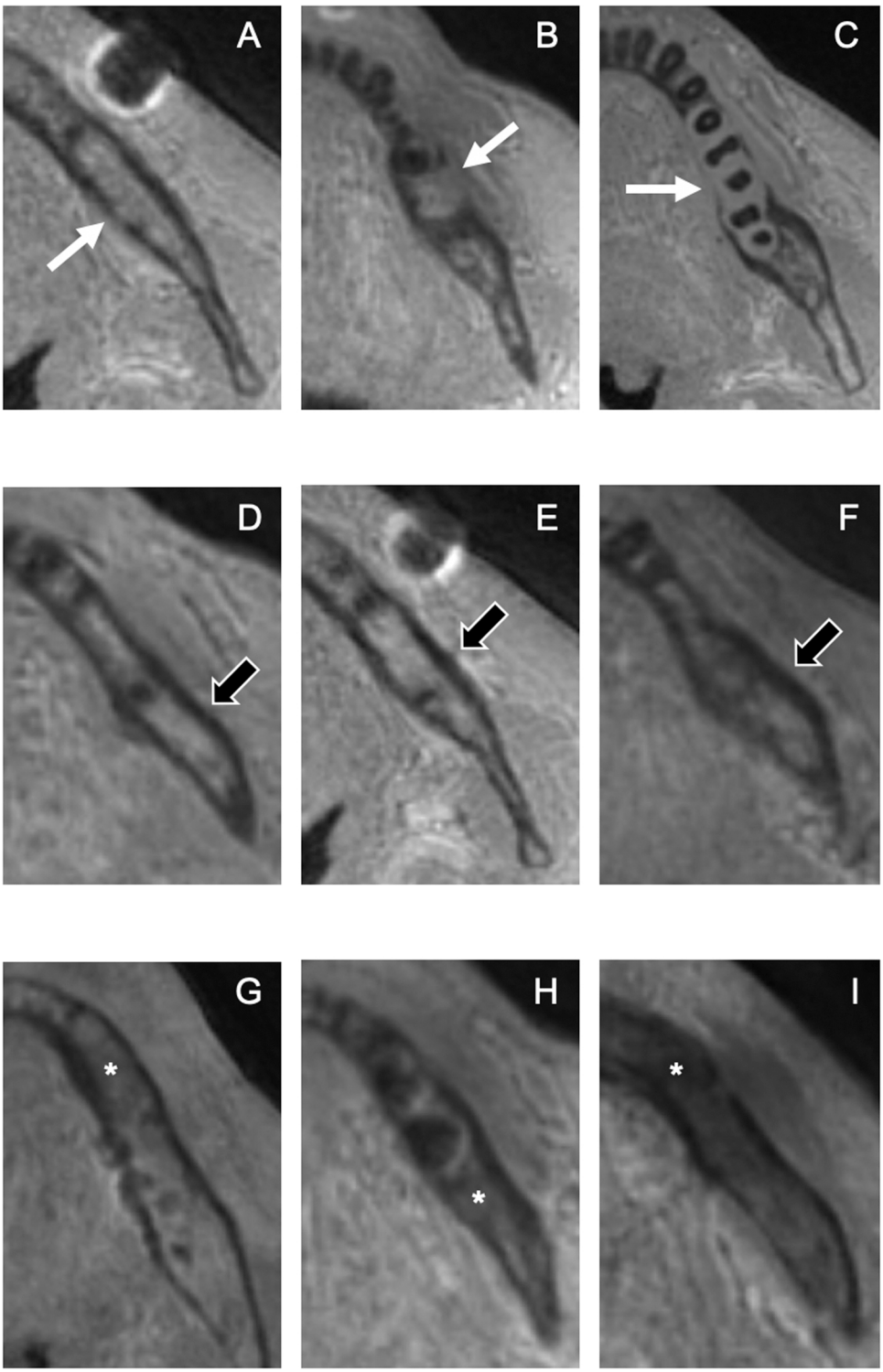

Fig. 1. Grading of pathological image findings in medication-related osteonecrosis of the jaw (MRONJ) on axial PETRA sequences with 60'000 radial acquisitions. Panels A-C show osteolysis (white arrows) in the right hemimandible with (A) slight thinning of the cortical bone (defined as "mild pathology"), (B) short discontinuity of cortical bone on one side of the jaw (defined as "moderate pathology"), and (C) extensive discontinuity of cortical bone on both sides of the jaw (defined as "severe pathology"). Panels D-F show different degrees of periosteal thickening (black arrows) with (D) slight (defined as "mild pathology"), (E) moderate (defined as "moderate pathology"), and (F) marked (defined as "severe pathology") thickening of the jaw cortex. Panels G-I show different degrees of medullary osteosclerosis (asterisks) with (G) slight (defined as "mild pathology"), (H) moderate (defined as "moderate pathology"), and (I) marked (defined as "severe pathology") hypointensity of the bone marrow according to visual impressions.

noted as such. In the healthy control group, overall bone delineation was assessed additionally using a 3-point Likert scale (1–3, for "sharp", "slightly blurred contour" defined as noisy bone cortex, and "markedly blurred contour" with a double contour).

The fast and ultra-fast PETRA sequences were qualitatively assessed in the same way with at least four weeks of time interval in between the readings. Visual hallmarks of MRONJ on standard, fast and ultra-fast PETRA sequences are shown in Fig. 2.

2.4. Quantitative analysis

Quantitative analysis was simultaneously performed in all PETRA sequences of the healthy control group by placing same-sized ROIs of 2 mm^2 (which accounts for approximately 10 pixels) in representative parts of healthy anatomic regions where the medullary bone was clearly visible (e.g., the condylar process, ramus of mandible, anterior and posterior mandible, alveolar mandibular corpus, and alveolar maxilla on both sides) and in air close to tissue in areas that were visually free of noise. The readers selected the same image slice on all three image series

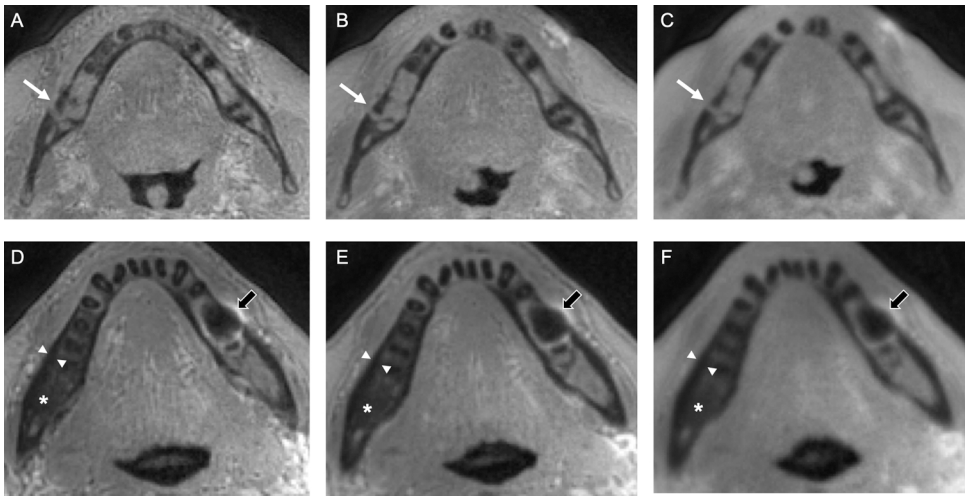

Fig. 2. Visual hallmarks of medication-related osteonecrosis of the jaw (MRONJ) on axial PETRA sequences with 60'000 (A, D), 30'000 (B, E) and 10'000 (C, F) radial acquisitions. Panels A-C show a right hemimandible affected by the disease featuring osteolysis (white arrows). Panels D-E show productive bony changes in a different patient as seen in MRONJ with diffuse medullary osteosclerosis (asterisks) and periosteal thickening/apposition (arrowheads). The qualitative MRONJ features are well visible throughout all sequences. Note the susceptibility artifact of dental hardware (black arrows) in the left hemimandible in panels D-E.

to perform the ROI measurements in the different regions. Mean and standard deviation (SD) values of signal intensity (SI) were calculated for each ROI.

To quantitatively assess image quality of the different PETRA sequences, contrast-to-noise ratios (CNR) were calculated in each sequence with the following formula:

$$CNR = \frac{mean\ \ SI\ \ of\ \ medullary\ \ bone\ \ in\ \ the\ \ condylar\ \ process - mean\ \ SI\ \ of\ \ masseter}{SD\ \ SI\ \ of\ \ air}$$

Additionally, image noise was assessed separately and the maximal bidirectional width of the biggest susceptibility artifact if present on each sequence was measured.

2.5. Statistical analysis

With regard to the interreader agreement for the detection of pathognomonic MRONJ-associated osteolytic lesions, diagnostic comparability between the PETRA sequences with 60'000, 30'000 and 10'000 RA was assessed by Cohen's kappa (κ). According to Landis and Koch [21], degrees of agreement were considered poor ($\kappa \leq 0$), slight ($0 < \kappa \leq 0.2$), fair ($0.2 < \kappa \leq 0.4$), moderate ($0.4 < \kappa \leq 0.6$), substantial ($0.6 < \kappa \leq 0.8$), or (almost) perfect ($0.8 < \kappa$). Bone delineation scores in the healthy control group were compared among different PETRA sequences using Wilcoxon signed-rank testing.

Sensitivity (SS), Specificity (SP), positive predictive value (PPV), negative predictive value (NPV), and accuracy were calculated, with the standard PETRA sequence of the more experienced reader serving as the reference standard since this sequence has previously been proven to distinguish diseased from normal bone with equal accuracy when compared to CBCT. [14] All statistical calculations were performed either by using the original measurements or by binary assessment of radiologically healthy (scores 0 and 1 on the previously mentioned 4-point Likert scale) versus clearly MRONJ-affected anatomic regions (scores 2 and 3).

Standard paired *t* testing and analysis of variances were performed for the assessment of differences in artifacts, CNR and image quality/noise between the sequences. For all measurements, a *P* value below 0.05 was considered significant. All calculations were performed using proprietary software (IBM SPSS Statistics, version 26; IBM, Armonk, NY).

3. Results

A total of 16 patients (6 males, 10 females, age 67.7 ± 12.9 years (mean ± SD)) and 16 healthy volunteers (8 males, 8 females, age 24.5 ± 2.9 years (mean ± SD)) received a total of 32 MR examinations according to the study protocol. In the MRONJ population, the majority of patients received denosumab (56%, n = 9), followed by BPs (25%, n = 4), and other drugs (19%, n = 3). The medications were most frequently administered to treat cancer-related conditions (56%, n = 9), followed by treatment of osteoporosis (25%, n = 4), and other conditions with altered bone turnover (19%, n = 3).

Acquisition times of the different PETRA sequences were reduced in all patients and volunteers from 315 to 165 and 65 s (60'000, 30'000, 10'000 RA, respectively).

3.1. Qualitative analysis

Comparison of qualitative parameters was performed in 229 of 288 (80%) predefined anatomic regions for osteolysis, in 226 of 288 (78%) regions for periosteal thickening, and in 221 of 288 (77%) regions for bone sclerosis. The remaining anatomic regions were rated as "non-diagnostic" by at least one reader due to susceptibility (mainly caused by metallic hardware in the oral cavity) or motion artifacts. Severe motion artifacts (rated as 2 or 3 on the Likert scale) were less frequent in the MR-sequences with a fewer number of RA (n = 2 in the fast PETRA-sequence; n = 1 in the ultra-fast PETRA-sequence) compared to the standard PETRA reference sequence (n = 7) (Fig. 3). Bone delineation was significantly different among PETRA sequences ($Z = -2.236$, $P = 0.025$ between standard and fast PETRA sequences; $Z = -3.419$, $P = 0.001$ between fast and ultra-fast PETRA sequences) with

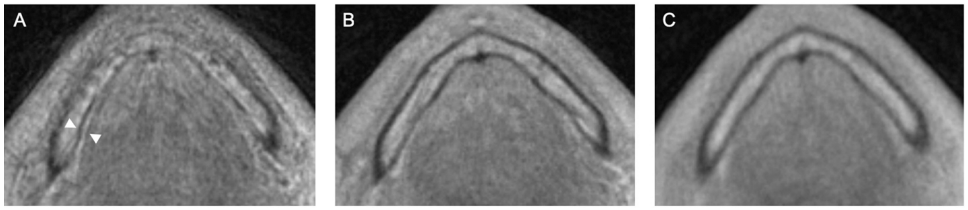

Fig. 3. Motion artifacts in relation to the number of radial acquisitions (RA) in PETRA imaging of the jaw. From left to right, sequences were acquired with (A) 60'000 RA, (B) 30'000 RA, and (C) 10'000 RA in a healthy volunteer. The standard PETRA reference sequence with 60'000 RA (A) shows severe distortion by motions artifacts with double-contouring (arrowheads) and non-diagnostic appearance of the cortical bone of the mandible. The fast (B) and ultrafast (C) PETRA sequences (30'000 and 10'000 RA, respectively) show almost no motion artifacts and allow for better assessment of the cortical bone.

Table 2a
Diagnostic performance of fast and ultra-fast PETRA imaging for the detection of osteolytic lesions compared to the standard PETRA reference sequence with 60'000 radial acquisitions.

	Standard PETRA (n = 16)	Fast PETRA (n = 16)	Ultra-fast PETRA (n = 16)
Osteolytic lesions (n)	23	20	17
Sensitivity	n/a	78%	74%
Specificity	n/a	99%	100%
Positive predictive value	n/a	90%	100%
Negative predictive value	n/a	98%	98%
Accuracy	n/a	98%	98%

PETRA indicates pointwise encoding time reduction with radial acquisition; Standard, fast and ultra-fast PETRA refers to the UTE MR bone imaging sequences with 60'000, 30'000 and 10'000 radial acquisitions, respectively. Results reported from the more experienced of the two readers.

Table 2b
Diagnostic performance of fast and ultra-fast PETRA imaging for the detection of productive bony changes (including periosteal thickening and bone sclerosis) compared to the standard PETRA reference sequence with 60'000 radial acquisitions.

	Standard PETRA (n = 16)	Fast PETRA (n = 16)	Ultra-fast PETRA (n = 16)
Productive bony changes (n)	48	42	44
Sensitivity	n/a	79%	71%
Specificity	n/a	99%	98%
Positive predictive value	n/a	90%	79%
Negative predictive value	n/a	98%	97%
Accuracy	n/a	98%	96%

PETRA indicates pointwise encoding time reduction with radial acquisition; Standard, fast and ultra-fast PETRA refers to the UTE MR bone imaging sequences with 60'000, 30'000 and 10'000 radial acquisitions, respectively. Results reported from the more experienced of the two readers.

increasingly blurred appearance when reducing the number of RA (Fig. 2).

Interreader agreement for the detection of osteolysis was moderate ($\kappa = 0.538$) when comparing the standard PETRA sequences, and fair ($\kappa = 0.227$ and $\kappa = 0.390$) when comparing the fast and ultra-fast PETRA sequences, respectively. SS, SP, PPV, NPV and accuracy for the detection of osteolytic lesions and productive bony changes (including periosteal thickening and bone sclerosis) in fast and ultra-fast PETRA imaging compared to the standard PETRA reference sequence are listed in Tables 2a and 2b.

3.2. Quantitative analysis

Measurements of quantitative parameters were performed in 131 of 160 (82%) predefined anatomic regions in the PETRA sequences of the healthy volunteers after exclusion of regions affected with susceptibility (mainly caused by metallic hardware in the oral cavity) or motion artifacts, predominantly affecting the anterior mandible and the alveolar mandibular corpus.

Assessment of CNR and image noise was possible in all examinations. CNR was 2.2 (mean; 95% CI 1.0 – 3.3) in the standard PETRA sequence, 1.9 (mean; 95% CI 1.2 – 2.6) in the fast PETRA sequence, and 2.2 (mean; 95% CI 1.3 – 3.1) in the ultra-fast PETRA sequence. There was no statistically significant difference between groups regarding CNR ($P = 0.846$).

Image noise was 38.1 (mean; 95% CI 31.0 – 45.3) in the standard PETRA sequence, 42.0 (mean; 95% CI 33.0 – 51.0) in the fast PETRA sequence, and 38.5 (mean; 95% CI 30.0 – 46.9) in the ultra-fast PETRA sequence. There was no statistically significant difference between groups regarding image noise ($P = 0.736$).

Susceptibility artifacts were present in 9 of 12 volunteers (75%). Maximal axial susceptibility artifact was 40.0 mm (mean; 95% CI 26.4 – 53.6 mm) in the standard PETRA sequence, 40.5 mm (mean; 95% CI 26.7 – 54.3 mm) in the fast PETRA sequence, and 40.3 mm (mean; 95% CI 26.4 – 54.2 mm) in the ultra-fast PETRA sequence. There was no statistically significant difference between groups regarding image artifacts ($P = 0.998$).

4. Discussion

The aim of this study was to assess the impact of decreasing number of RA in order to accelerate a UTE MR bone imaging sequence on bone depiction quality in MRONJ. Image quality of each sequence was comparable regarding CNR, image noise and artifact dimensions despite decreasing sharpness of bone contours with increasing acceleration of acquisitions. However, no significant trade-off in terms of diagnostic performance was noted with high accuracy of the fast and ultra-fast PETRA sequences (96 – 98%) for the detection of osteolytic lesions and productive bony changes compared to the standard PETRA reference sequence.

Although initially described for bisphosphonate treatment, the majority of study subjects in this cohort (56%) developed the disease after administration of denosumab for the treatment of cancer-related conditions, which is also concordant with other study cohorts [22]. Mean patient age of 68 years and a slight female predominance (63%) also correspond well to published reports on typical MRONJ demographics [23].

To this day, the definition of MRONJ according to a position paper of the AAOMS does not contain imaging-related criteria [1]. However, in current clinical practice panoramic radiographs and CBCT are often used to assess characteristic alterations of diseased bone [24]. The disadvantage of those modalities is the use of ionizing radiations, and the lack of assessment of surrounding soft tissues that may also be affected by the disease in advanced stages [12]. MR imaging is known for its optimal

soft tissue contrast and thus assessment of soft tissues in the head and neck region. Recently, several groups have used similar UTE MR bone imaging sequences of different vendors to detect structures with very short echo times such as tendons and bones. [13–15,25–27] Qualitative assessment of MRONJ with UTE MR imaging has proven to be comparable to the reference standard CBCT, and quantitative measurements of both modalities were able to significantly distinguish diseased from normal bone with strong correlations among each other [14].

However, MR imaging is susceptible to motion artifacts since image acquisition times are substantially longer compared to conventional radiographs or CBCT. This may become a problem, especially in the predominantly older MRONJ patient population due to inability to lay down for an extended period of time. Acceleration of image acquisition, e.g. by reducing the number of RA in a PETRA sequence, can lead to shorter acquisition times which should result in a fewer number of severe motion artifacts. This could be confirmed in this study: fewer RA led to a significant shortening of respective acquisition times. Accordingly, a significant reduction of severe motion artifacts was noted while the size of susceptibility artifacts due to dental hardware remained largely unchanged.

Other quantitative parameters such as CNR and image noise remained unchanged when comparing standard, fast and ultra-fast PETRA sequences. This can be explained as a consequence of fundamental MR image formation principles. Most MR image information (e.g. contrast and general shape) is contained in the center of the k-space. Spatial resolution on the other hand is encoded primarily in the periphery [28]. Thus, by radially collecting data from the k-space, contrast remains rather unchanged when lowering the number of RA. Spatial resolution, however, impairs with fewer RA which is consistent with our data and visual impressions. Bone delineation significantly decreased and became more blurred with increasing acceleration, i.e. reduction of RA. However, pathologic bone changes such as subtle sclerotic or osteolytic lesions were not affected to the same extent.

In contrast to differences in bone delineation, a similar diagnostic performance of the fast and ultra-fast PETRA sequences was noted with high accuracy (96 – 98%) for the detection of MRONJ induced osteolytic lesions and productive bony changes alike compared to the standard PETRA reference sequence. Only the PPV for significant productive bone changes decreased from 90% to 79% when comparing fast to ultra-fast PETRA images. Nevertheless, this may indeed be due to a certain loss of bone delineation with markedly accelerated image acquisitions.

However, interreader agreement for the detection of pathognomonic osteolysis decreased from moderate to fair when comparing PETRA sequences with a fewer number of RA. The authors attribute this mostly to the different number of years of experience of the two readers (3 and 13 years, respectively) since MRONJ is a disease that younger, non-subspecialized radiologists do not encounter often in their training. Clinical experience is thus certainly important in correctly assessing bony lesions associated with MRONJ.

There are limitations to this study. First, although MRONJ is increasing in incidence in the Western World, it is still a relatively rare disease entity. Hence, the patient group consisted of only 16 patients. However, the authors believe that study findings and conclusions are sufficiently supported despite the limited number of patients included. Second, differences in spatial resolution between MR sequences with different numbers of RA were only assessed qualitatively but not quantitatively. One could imagine that subtle bony changes in the early stages of MRONJ would be missed when assessing them with PETRA sequences with 30'000 or 10'000 RA as compared to sequences with 60'000 RA. However, in patients with clinically confirmed MRONJ with bone exposure (more advanced stage of disease), we did not experience any disadvantage of disease assessment in MR images with a fewer number of RA. Last, we assessed a vendor-specific UTE MR bone imaging sequence, i.e. PETRA, and the respective impact of reducing RA in order to accelerate image acquisition. Alternative acceleration techniques in different UTE MR sequences may have a different impact on the diagnostic accuracy of bone changes in MRONJ.

5. Conclusions

UTE MR bone imaging sequences with a lower number of RA provide sufficient image quality for detecting osteolytic lesions and productive bony changes in MRONJ subjects at faster acquisition times compared to the respective standard UTE MR bone imaging sequence.

Funding statement

This research did not receive any specific grant from funding agencies in the public, commercial, or not-for-profit sectors.

Ethical statement

This study was approved by the institutional review board and the local ethics committee and conducted in accordance with the principles of the Declaration of Helsinki. Written general consent for the use of clinical data for scientific purposes was obtained from each patient.

CRediT authorship contribution statement

J.M.G: Conceptualization, Data curation, Formal analysis, Investigation, Methodology, Writing – original draft. **F.A.H:** Conceptualization, Data curation, Formal analysis, Investigation, Methodology, Writing – original draft. **D.N:** Data curation, Investigation, Writing – review & editing. **E.D.C:** Data curation, Investigation, Writing – review & editing. **P.S:** Conceptualization, Resources, Writing – review & editing. **T.F.:** Conceptualization, Writing – review & editing. **F.D.G:** Conceptualization, Writing – review & editing. **R.G:** Conceptualization, Methodology, Project administration, Resources, Supervision, Writing – review & editing.

Declaration of Competing Interest

The authors declare that they have no known competing financial interests or personal relationships that could have appeared to influence the work reported in this paper.

References

[1] S.L. Ruggiero, T.B. Dodson, J. Fantasia, R. Goodday, T. Aghaloo, B. Mehrotra, F. O'Ryan, American Association of Oral and Maxillofacial Surgeons, American Association of Oral and Maxillofacial Surgeons position paper on medication-related osteonecrosis of the jaw–2014 update, J. Oral. Maxillofac. Surg. 72 (2014) 1938–1956, https://doi.org/10.1016/j.joms.2014.04.031.

[2] F. Hallmer, G. Andersson, B. Götrick, G. Warfvinge, J. Anderud, T. Bjørnland, Prevalence, initiating factor, and treatment outcome of medication-related osteonecrosis of the jaw-a 4-year prospective study, Oral Surg. Oral Med. Oral Pathol. Oral Radiol. 126 (2018) 477–485, https://doi.org/10.1016/j.oooo.2018.08.015.

[3] S.R. Cummings, J. San Martin, M.R. McClung, E.S. Siris, R. Eastell, I.R. Reid, P. Delmas, H.B. Zoog, M. Austin, A. Wang, S. Kutilek, S. Adami, J. Zanchetta, C. Libanati, S. Siddhanti, C. Christiansen, FREEDOM Trial, Denosumab for prevention of fractures in postmenopausal women with osteoporosis, N. Engl. J. Med. 361 (2009) 756–765, https://doi.org/10.1056/NEJMoa0809493.

[4] P. Major, A. Lortholary, J. Hon, E. Abdi, G. Mills, H.D. Menssen, F. Yunus, R. Bell, J. Body, E. Quebe-Fehling, J. Seaman, Zoledronic acid is superior to pamidronate in the treatment of hypercalcemia of malignancy: a pooled analysis of two randomized, controlled clinical trials, J. Clin. Oncol. 19 (2001) 558–567, https://doi.org/10.1200/JCO.2001.19.2.558.

[5] L.S. Rosen, D. Gordon, N.S. Tchekmedyian, R. Yanagihara, V. Hirsh, M. Krzakowski, M. Pawlicki, P. De Souza, M. Zheng, G. Urbanowitz, D. Reitsma, J. Seaman, Long-term efficacy and safety of zoledronic acid in the treatment of skeletal metastases in patients with nonsmall cell lung carcinoma and other solid tumors: a randomized, Phase III, double-blind, placebo-controlled trial, Cancer 100 (2004) 2613–2621, https://doi.org/10.1002/cncr.20308.

[6] D.H. Henry, L. Costa, F. Goldwasser, V. Hirsh, V. Hungria, J. Prausova, G. V. Scagliotti, H. Sleeboom, A. Spencer, S. Vadhan-Raj, R. von Moos, W. Willenbacher, P.J. Woll, J. Wang, Q. Jiang, S. Jun, R. Dansey, H. Yeh, Randomized, double-blind study of denosumab versus zoledronic acid in the treatment of bone metastases in patients with advanced cancer (excluding breast

and prostate cancer) or multiple myeloma, J. Clin. Oncol. 29 (2011) 1125–1132, https://doi.org/10.1200/JCO.2010.31.3304.
[7] F. Saad, J.E. Brown, C. Van Poznak, T. Ibrahim, S.M. Stemmer, A.T. Stopeck, I. J. Diel, S. Takahashi, N. Shore, D.H. Henry, C.H. Barrios, T. Facon, F. Senecal, K. Fizazi, L. Zhou, A. Daniels, P. Carrière, R. Dansey, Incidence, risk factors, and outcomes of osteonecrosis of the jaw: integrated analysis from three blinded active-controlled phase III trials in cancer patients with bone metastases, Ann. Oncol. 23 (2012) 1341–1347, https://doi.org/10.1093/annonc/mdr435.
[8] A. Krishnan, A. Arslanoglu, N. Yildirm, R. Silbergleit, N. Aygun, Imaging findings of bisphosphonate-related osteonecrosis of the jaw with emphasis on early magnetic resonance imaging findings, J. Comput. Assist. Tomogr. 33 (2009) 298–304, https://doi.org/10.1097/RCT.0b013e31817e4986.
[9] F. Wilde, M. Heufelder, K. Lorenz, S. Liese, J. Liese, J. Helmrich, A. Schramm, A. Hemprich, E. Hirsch, K. Winter, Prevalence of cone beam computed tomography imaging findings according to the clinical stage of bisphosphonate-related osteonecrosis of the jaw, Oral Surg. Oral Med. Oral Pathol. Oral Radiol. 114 (2012) 804–811, https://doi.org/10.1016/j.oooo.2012.08.458.
[10] P. Stockmann, F.M. Hinkmann, M.M. Lell, M. Fenner, E. Vairaktaris, F.W. Neukam, E. Nkenke, Panoramic radiograph, computed tomography or magnetic resonance imaging. Which imaging technique should be preferred in bisphosphonate-associated osteonecrosis of the jaw? A prospective clinical study, Clin. Oral. Investig. 14 (2010) 311–317, https://doi.org/10.1007/s00784-009-0293-1.
[11] W. De Vos, J. Casselman, G.R. Swennen, Cone-beam computerized tomography (CBCT) imaging of the oral and maxillofacial region: a systematic review of the literature, Int. J. Oral. Maxillofac. Surg. 38 (2009) 609–625, https://doi.org/10.1016/j.ijom.2009.02.028.
[12] R. Guggenberger, D.R. Fischer, P. Metzler, G. Andreisek, D. Nanz, C. Jacobsen, D. T. Schmid, Bisphosphonate-induced osteonecrosis of the jaw: comparison of disease extent on contrast-enhanced MR imaging, [18F] fluoride PET/CT, and conebeam CT imaging, AJNR Am. J. Neuroradiol. 34 (2013) 1242–1247, https://doi.org/10.3174/ajnr.A3355.
[13] E.Y. Chang, J. Du, C.B. Chung, UTE imaging in the musculoskeletal system, J. Magn. Reson. Imaging 41 (2015) 870–883, https://doi.org/10.1002/jmri.24713.
[14] F.A. Huber, P. Schumann, J. von Spiczak, M.C. Wurnig, M. Klarhöfer, T. Finkenstaedt, A. Bedogni, R. Guggenberger, Medication-related osteonecrosis of the jaw-comparison of bone imaging using ultrashort echo-time magnetic resonance imaging and cone-beam computed tomography, Investig. Radio. 55 (2020) 160–167, https://doi.org/10.1097/RLI.0000000000000617.
[15] E. Deininger-Czermak, C. Villefort, N. von Knebel Doeberitz, S. Franckenberg, P. Kälin, D. Kenkel, D. Gascho, M. Piccirelli, T. Finkenstaedt, M.J. Thali, R. Guggenberger, Comparison of MR ultrashort echo time and optimized 3D-multiecho in-phase sequence to computed tomography for assessment of the osseous craniocervical junction, J. Magn. Reson. Imaging 53 (2021) 1029–1039, https://doi.org/10.1002/jmri.27478.
[16] D.M. Grodzki, P.M. Jakob, B. Heismann, Ultrashort echo time imaging using pointwise encoding time reduction with radial acquisition (PETRA), Magn. Reson. Med. 67 (2012) 510–518, https://doi.org/10.1002/mrm.23017.
[17] V.M. Runge, J.K. Richter, J.T. Heverhagen, Motion in magnetic resonance: new paradigms for improved clinical diagnosis, Investig. Radio. 54 (2019) 383–395, https://doi.org/10.1097/RLI.0000000000000566.
[18] L. Hu, K.H. Su, G.C. Pereira, A. Grover, B. Traughber, M. Traughber, R.F. Muzic Jr, k-space sampling optimization for ultrashort TE imaging of cortical bone: applications in radiation therapy planning and MR-based PET attenuation correction, Med. Phys. 41 (2014), 102301, https://doi.org/10.1118/1.4894709.
[19] R. Likert, A technique for the measurements of attitudes, Arch. Psychol. 140 (1932) 5–55.
[20] P. Schumann, S. Morgenroth, F.A. Huber, N.J. Rupp, F. Del Grande, R. Guggenberger, Correlation of dynamic contrast-enhanced bone perfusion with morphologic ultra-short echo time MR imaging in medication-related osteonecrosis of the jaw, Dentomaxillofac. Radiol. 51 (2022) 20210036, https://doi.org/10.1259/dmfr.20210036.
[21] J.R. Landis, G.G. Koch, The measurement of observer agreement for categorical data, Biometrics 33 (1977) 159–174.
[22] W.X. Qi, L.N. Tang, A.N. He, Y. Yao, Z. Shen, Risk of osteonecrosis of the jaw in cancer patients receiving denosumab: a meta-analysis of seven randomized controlled trials, Int. J. Clin. Oncol. 19 (2014) 403–410, https://doi.org/10.1007/s10147-013-0561-6.
[23] M. El-Rabbany, A. Sgro, D.K. Lam, P.S. Shah, A. Azarpazhooh, Effectiveness of treatments for medication-related osteonecrosis of the jaw: a systematic review and meta-analysis, J. Am. Dent. Assoc. 148 (2017) 584–594, https://doi.org/10.1016/j.adaj.2017.04.002.
[24] R. Guggenberger, E. Koral, W. Zemann, C. Jacobsen, G. Andreisek, P. Metzler, Cone beam computed tomography for diagnosis of bisphosphonate-related osteonecrosis of the jaw: evaluation of quantitative and qualitative image parameters, Skelet. Radio. 43 (2014) 1669–1678, https://doi.org/10.1007/s00256-014-1951-1.
[25] C.S. Rajapakse, M. Bashoor-Zadeh, C. Li, W. Sun, A.C. Wright, F.W. Wehrli, Volumetric cortical bone porosity assessment with MR imaging: validation and clinical feasibility, Radiology 276 (2015) 526–535, https://doi.org/10.1148/radiol.15141850.
[26] Y.J. Ma, J. West, A. Nazaran, X. Cheng, H. Hoenecke, J. Du, E.Y. Chang, Feasibility of using an inversion-recovery ultrashort echo time (UTE) sequence for quantification of glenoid bone loss, Skelet. Radio. 47 (2018) 973–980, https://doi.org/10.1007/s00256-018-2898-4.
[27] T. Finkenstaedt, P. Siriwanarangsun, S. Achar, M. Carl, S. Finkenstaedt, N. Abeydeera, C.B. Chung, W.C. Bae, Ultrashort time-to-echo magnetic resonance imaging at 3 T for the detection of spondylolysis in cadaveric spines: comparison with CT, Investig. Radio. 54 (2019) 32–38, https://doi.org/10.1097/RLI.0000000000000506.
[28] C.B. Paschal, H.D. Morris HD, K-space in the clinic, J. Magn. Reson. Imaging 19 (2004) 145–159, https://doi.org/10.1002/jmri.10451.